ISSN 0016-7932, Geomagnetism and Aeronomy, 2018, Vol. 58, No. 4, pp. 469–482. © Pleiades Publishing, Ltd., 2018.
Original Russian Text © T.A. Popova, A.G. Yahnin, A.G. Demekhov, S.A. Chernyaeva, 2018, published in Geomagnetizm i Aeronomiya, 2018, Vol. 58, No. 4, pp. 484–497.

# Generation of EMIC Waves in the Magnetosphere and Precipitation of Energetic Protons: Comparison of the Data from THEMIS High Earth Orbiting Satellites and POES Low Earth Orbiting Satellites

**T. A. Popova[a] *, A. G. Yahnin[a], A. G. Demekhov[a, b], and S. A. Chernyaeva[c]**

[a] *Polar Geophysical Institute, Apatity, Russia*
[b] *Institute of Applied Physics, Russian Academy of Sciences, Nizhny Novgorod, Russia*
[c] *St. Petersburg State University, St. Petersburg, Russia*
**e-mail: tarkada@yandex.ru*

Received October 25, 2017

**Abstract**—Regions of the detection of electromagnetic ion-cyclotron (EMIC) waves on the THEMIS satellites near the equatorial plane and the precipitation of energetic protons on POES low Earth orbiting satellites are compared with the magnetospheric magnetic field model. It is confirmed that low Earth orbiting satellites detect the precipitation of energetic protons in the regon associated with observations of EMIC waves in the magnetosphere. This is consistent with the idea that protons are scattered in the loss cone as a result of ion-cyclotron interaction. Thus, observations of fluxes of energetic protons in low Earth orbits can be used to monitor ion-cyclotron instability regions in the magnetosphere. Simultaneous observations at high and low Earth orbits contribute to the construction of a spatiotemporal pattern of the interaction region of EMIC waves and energetic protons. In addition, it is shown that proton precipitation associated with EMIC waves can cause errors in determining the latitude of the isotropic boundary (the equatorial boundary of isotropic fluxes of energetic protons), which is an indicator of the configuration of the magnetic field in the magnetosphere.

**DOI:** 10.1134/S0016793218040114

## 1. INTRODUCTION

The ion-cyclotron (IC) instability increment and the generation of electromagnetic ion-cyclotron (EMIC) waves directly depends on the density of energetic protons and the presence of their transverse pitch angle anisotropy (Sagdeev and Shafranov, 1960; Kennel and Petschek, 1966). Thus, the ring current region in the near-Earth magnetosphere is a very suitable place for generating EMIC waves. The theory states (Kennel and Petschek, 1966; Coroniti et al., 1970; Bespalov et al., 1994) that ions (mostly protons) of the ring current are scattered over the pitch angles when interacting with EMIC waves. Some of these ions end up in the loss cone and precipitate into the Earth's atmosphere. An experimental study of the relationship between the filling of the loss cone and EMIC waves, which obviously should involve in their simultaneous observation and comparison of their parameters, is an important problem, because it not only confirms the theory but also makes it possible to identify regions of the development of IC instability based on observations of fluxes of energetic protons. The theory makes it possible to estimate the energy of waves in the magnetosphere by measured fluxes of energetic charged particles precipitating into the ionosphere. There have also been attempts to test these ratios with the use of satellite data (for whistler waves and energetic electrons, for example (Li et al., 2014).

Unfortunately, it is rather difficult to organize such an experiment and interpret the results of observations. For magnetospheric equatorial satellites, the angular resolution of particle sensors is often greater than the loss cone (i.e., it is impossible to distinguish between trapped and precipitating particles). There are only a few papers in which EMIC waves were compared to filling a loss cone based on observations on a single spacecraft. Thus, Erlandson and Ukhorsky (2001) considered three EMIC wave events that were detected by the Dynamics Explorer-1 satellite. During these events, there was an increase in the flux of protons with energies of 0.2–17 keV in the loss cone. Yahnin and Yahnina (2007) and Yahnin et al. (2001), according to the data of the POLAR satellite, considered an event in which EMIC waves correlated with the filling of the loss cone with 30-keV protons. Both of these studies used satellites that were located quite far from the equatorial plane so that the loss cone was large enough for the particle sensor to detect it.

Low Earth orbiting satellites, for which the loss cone is large (tens of degrees) and can exceed the angular resolution of particle sensors, are rarely equipped with both wave and particle sensors simulta-

neously. At the same time, particle precipitation on such satellites can be compared with measurements of waves on other spacecraft. Such comparisons have already been made, although they are also extremely rare. For example, Morley et al. (2009) showed the interconnection of EMIC waves on the GOES-9 satellite with precipitations of >10 keV protons on the DMSP F-13 satellite. Usanova et al. (2010) demonstrated such a relationship by comparing observations of energetic protons on the NOAA-17 satellite with observations of waves in the subequatorial magnetosphere on the Cluster satellite.

Yahnina et al. (2003) statistically compared the data from NOAA POES low Earth orbiting satellites on proton precipitation with observations of geomagnetic pulsations in the *Pc*1 (0.1–5 Hz) range at the Sodankylä ground station. These pulsations are considered an indicator of EMIC waves. A high correlation was found between pulsations and bursts of precipitation of energetic protons within the anisotropic zone (the region where the low Earth orbiting satellite sees mainly the predominance of captured fluxes over the precipitating ones). At the same time, this correlation is not direct proof that the waves and the scattering of particles originate from the same source, because the ground measurements of geomagnetic pulsations at one station do not make it possible to localize the source of pulsations. Semenova et al. (2017) used the NOAA POES data to construct a global probability distribution of proton precipitation in an anisotropic zone, which turned out to be similar to the observation probability distribution of EMIC waves obtained from satellite data in the magnetosphere (for example, Usanova et al., 2012).

In this paper, we will try to expand the statistics of "direct" comparisons of proton precipitations with EMIC waves based on simultaneous and conjugate observations of waves in the subequatorial magnetosphere from the THEMIS satellites and proton precipitation from POES (NOAA and MetOp) low Earth orbiting satellites.

## 2. DATA, SELECTION, AND PROCESSING OF EVENTS

Low-frequency magnetic field fluctuations in the near-Earth plasma were detected by flux gate magnetometers (FGMs) (Auster et al., 2008) of three magnetospheric THEMIS satellites-A, -D, and -E (TH-A, TH-D, and TH-E) (Angelopoulos, 2008). The elliptical orbit of these satellites is arranged in such a way that they move successively, one after the other, along close trajectories near the equatorial plane of the magnetosphere. The apogee of the orbits of these satellites was at $12–13R_E$. The FGM detects three components of the magnetic field vector. In this paper, we used data with a polling frequency of 4 Hz.

Fluxes of precipitating particles including energetic protons were measured by POES satellites (NOAA-15, -16, -17, -18, -19, and MetOp-2). These satellites have a circular polar orbit with an altitude of ~800 km. Particles with energies of >30 keV are measured by the Medium Energy Proton and Electron Detector (MEPED) (Evans and Greer, 2004), which has two pairs of orthogonal particle sensors (one pair for protons, the other for electrons). In each pair of sensors, one of them is directed vertically to the zenith, and the other is directed back along the trajectory of the satellite. The loss cone at this altitude is about 60°, while the aperture of the device is 30°. Thus, at sufficiently high $L$-shells (we are interested in the regions above $L = 3$), the vertical sensor measures the precipitating particles and the second measures the trapped particles. The Total Energy Detector (TED) (Evans and Greer, 2004), which measures only precipitating particles, is used to detect particles with energies below 20 keV. The temporal resolution of particle detection is 2 s. The orbital period of the NOAA POES satellites is about 2 h. These satellites cross the region of latitudes in which precipitations of energetic charged particles are usually observed in a few minutes.

Space Physics Environment Data Analysis Software (SPEDAS) (http://themis.ssl.berkeley.edu/software.shtml), which consists of subprograms in the Interactive Data Language (IDL) environment was used to process the data of the above satellite instruments. This software makes it possible to download data in the Common Data Format (CDF) and to analyze and visualize them; it also supports the simultaneous processing of data from several missions. The GEOPACK library (http://ampere.jhuapl.edu/code/idl_geopack.html) was adapted for the IDL. This library makes it possible to plugin magnetospheric magnetic field models of N.A. Tsyganenko, which are necessary to project satellites into the magnetosphere and ionosphere. Such projection is of fundamental importance for the comparison of measurements by satellites located at such different altitudes. Since the list of SPEDAS plugins does not include the POES mission, additional programs have been developed to download, analyze, and visualize the data from these satellites, and, using the coordinates of the satellite's trajectory, to project its position to the equatorial plane and to ionospheric heights.

Invariant coordinates were used to compare data from different satellites. In order to calculate the invariant latitude of the satellite, its position was projected along the magnetic field line in the IGRF+T89 model (combination of the Earth's main field model (https://www.ngdc.noaa.gov/IAGA/vmod/igrf.html) and the Tsyganenko model (Tsyganenko, 1989) for the description of the field of external sources) to the most remote point on this line. Then, using the formula $L = 1/\cos^2(a)$, we determined the invariant latitude $a$, where $L$ is the distance from the Earth (in Earth radii) to the magnetospheric projection of the satellite. The

calculation by this formula is similar to the projection from a point on the equatorial plane to the Earth along the line of force of a dipole magnetic field. The MLT value (in hours), the second coordinate of the polar coordinate system, is calculated by the formula $MLT = (12/\pi)\arctan(y_{SM}/x_{SM})$, where $y_{SM}$ and $x_{SM}$ are the coordinates of the satellite trajectory to the Earth in the SM coordinate system. Such calculations were carried out for both magnetospheric and low Earth orbiting satellites. It should be noted that the T89 model is parametrized by the *Kp* geomagnetic activity index, which characterized the geomagnetic activity during the periods of magnetic field measurements to construct the model. The model was constructed for the mean values of the magnetic field, and the characteristics of the field can differ in specific situations with the same *Kp*. For definiteness, the calculation for each event was carried out for the version of the model that corresponded to the value of the *Kp* index actually observed in the event.

Events for the analysis were selected based on spectrograms from the FGM on the THEMIS website (http://themis.ssl.berkeley.edu). Well-defined events with a duration of at least half an hour were selected when emissions were observed in the spectrograms of the magnetic field at frequencies below the hydrogen gyrofrequency and the transverse component (with respect to the direction of the vector of the total magnetic field) of these fluctuations was much more intense than the longitudinal component. Such properties are characteristic of EMIC waves. Then, the part of the THEMIS trajectory on which the waves were detected, as well as the trajectories of the POES satellites during wave detection, was converted in the invariant latitude–MLT coordinate system. Passages selected for the analysis met the following criteria: (1) the trajectory of the low Earth orbiting satellite should cross the region of latitudes at which EMIC waves are observed and (2) the longitudinal difference between the trajectories of the THEMIS and POES satellites should not be more than 1 h MLT at these latitudes.

In order to compare data from different satellites, latitudinal profiles of the corresponding parameters were constructed for each of them along, with the projection of the trajectories of satellites on the invariant latitude–MLT plane. According to the FGM data, the maximum intensities of EMIC waves were calculated for the THEMIS satellites in two characteristic frequency bands: $f_{He^+} < f < f_{H^+}$ ($H^+$ band) and $f_{O^+} < f < f_{He^+}$ ($He^+$ band), where $f_{He^+}$, $f_{O^+}$ are the gyrofrequencies of hydrogen, helium, and oxygen ions. The gyrofrequencies were determined based on measurements of the total magnetic field by the FGM. The latitudinal profiles of fluxes of trapped and precipitating protons in the energy range 30–80 keV (according to the MEPED) and, in some cases, the energy flux of precipitating protons with energies of <20 keV (according to the TED) were constructed for POES satellites. For 2007–2009, 157 events were selected for analysis. In this paper, we discuss in detail the results for several events and give statistical results for all events.

## 3. RESULTS

### *3.1. Analysis of Individual Events*

#### *3.1.1. Event of July 14, 2009*

Ion-cyclotron waves were detected by the TH-E satellite in the interval of 1550–1700 UT at a frequency of 0.2–0.4 Hz in the $He^+$ band at a distance from the Earth of 5.5–7$R_E$ and ~14 MLT (Fig. 1). TH-A and TH-D satellites crossed this region about 1.5 h and 1 h earlier, respectively, and no waves were detected. Figure 2 shows the projections of TH-E satellite orbits for the interval of 1530–1728 UT and the trajectories of the NOAA-18 satellite passages in the Northern Hemisphere in the interval of 1554–1600 UT, the NOAA-19 satellite in the Southern Hemisphere in the interval of 1632-1638 UT, and the NOAA-18 satellite in the Southern Hemisphere in the interval of 1655-1701 UT. The position of the TH-E satellite during the passage of the low Earth orbiting satellite almost did not change; it is marked by a dot. Figures 3a and 3b show the dependence of the maximum spectral intensity of EMIC waves on latitude in two bands ($H^+$ and $He^+$, respectively). The waves in the $He^+$ band are much more intense than in the $H^+$ band. The region in which TH-E detected EMIC waves takes about three degrees of latitude (65°–68° InvLat) and almost 2 h for MLT. The three pairs of vertical (solid, dashed, and dotted) lines in Figs. 1a and 1b show the latitude intervals in which the TH-E projection was located during the NOAA-18 and -19 satellite passages. Figs. 3c, 3d, and 3e show the latitudinal profiles of proton fluxes with energies of 30–80 keV of these satellites. During the passage of the NOAA-18 satellite in the Northern Hemisphere (~1554–1600 UT), the TH-E satellite was in the latitude interval indicated by the two vertical dotted lines in Figs. 3a and 3b and had not yet entered the EMIC wave generation region. Accordingly, no proton precipitations of significant intensity were detected at these latitudes, but they are detected at higher latitudes (Fig. 3c), where later the TH-E satellite observed EMIC waves.

The NOAA-19 satellite crossed the latitude region of 60°–75° InvLat at ~1631–1637 UT. At that time, the TH-E satellite was in the latitude range marked by two vertical solid lines in Figs. 3a and 3b and detected quite intense EMIC waves. The NOAA-19 satellite observed proton precipitation at both the TH-E projection latitude and almost in the entire latitude range where TH-E observed EMIC waves (Fig. 3d).

The NOAA-18 passage in the Southern Hemisphere at ~1655–1701 UT occurred when the TH-E satellite detected a decrease in the EMIC wave inten-

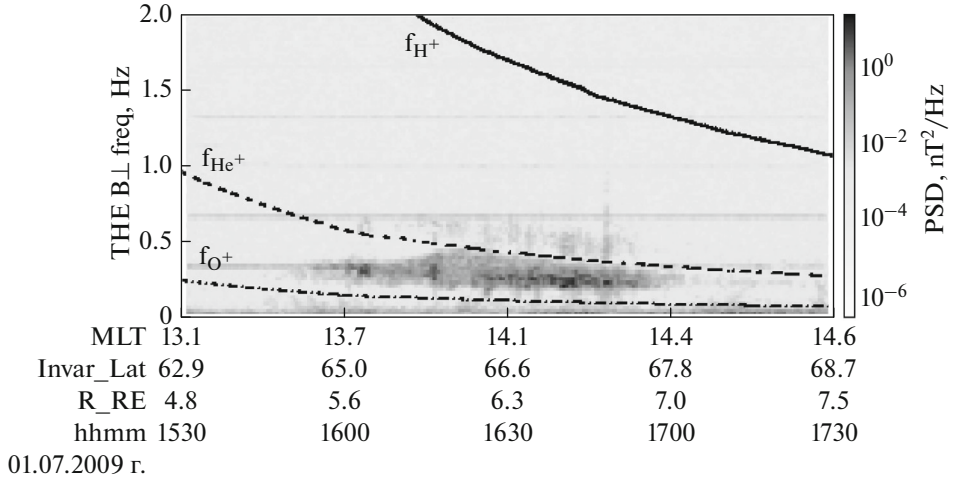


**Fig. 1.** Spectrogram of transverse fluctuations of the magnetic field measured by the THEMIS-E satellite at 1530–1730 UT on July 1, 2009. Solid, dashed, and dot-dash lines show the gyrofrequencies of hydrogen, helium, and oxygen ions, respectively.

sity (or the satellite was leaving the EMIC wave generation region). During this passage of the low orbiting satellite, TH-E was at latitudes marked with vertical dashed lines. The precipitations detected by the NOAA-18 satellite during this passage occupy a small range of latitudes and have a much lower intensity compared with measurements of NOAA-19 (Fig. 3e).

The data shown in Fig. 3 obviously correlate with concepts that the precipitation of energetic protons is associated with the scattering of particles by EMIC waves. In general, the latitudinal extent of proton precipitation corresponds to the extent of the region where EMIC waves were detected. The variability of the region of proton precipitations and variations in their intensity, which can be seen in the data of successive passages of low Earth orbiting satellites, do not contradict these concepts. Indeed, when interpreting observations of EMIC waves by a magnetospheric satellite near the equatorial plane and comparing them with fluxes of energetic protons at low altitudes, one must take into account the fact that the magnetospheric satellite crosses the wave generation region for a rather long time (in the considered example, for more than 1 h). Obviously, the wave intensity variations observed in this case are a superposition of both spatial and temporal variations. At the same time, a low Earth orbiting satellite crosses the projection of the wave generation region in a time of the order of 1 min. If the precipitation of energetic protons is associated with the scattering of particles by EMIC waves, the latitudinal distribution of the precipitations displays the instantaneous position of the EMIC wave region, and changes in this distribution from passage to passage of the low Earth orbiting satellite display temporary variations in the EMIC wave region.

### *3.1.2. Events of June 6, 2009*

On this day, there were two intervals of observations of EMIC waves. In the interval of 1230–1315 UT, the TH-A satellite crossed the generation region of EMIC waves in the $He^+$ band, at MLT = ~16 at a distance from the Earth of ~6.5–7$R_E$. The NOAA-15 low Earth orbiting satellite crossed the projection of this region at ~1247 UT and detected an isolated burst of precipitations of energetic protons. Figure 4 illustrates this event. It can be seen that the regions of precipitation of protons and generation of EMIC waves approximately coincide.

TH-D and TH-E satellites moved along almost the same trajectory as the TH-A satellite but lagged behind it by 6 and 7 h, respectively. In the evening sector, both satellites detected EMIC waves at ~1630–1730 MLT, but at different times (1815–1840 and 1900–1930 UT, respectively) and at different distances from the Earth (6.5–7$R_E$ and 8.5–8.9$R_E$, respectively) (Fig. 5). Because of the impossibility to unambiguously separate spatial variations from temporal variations even in the presence of two magnetospheric satellites, it is rather difficult to determine whether the detection of waves by satellites is a manifestation of the evolution of one wave generation region or wether there were two such regions.

For more information, consider the data from POES low Earth orbiting satellites, the passages of which met the aforementioned criteria for selecting conjugate events. Figures 6–11 on the left show a map with TH-D and TH-E trajectories and with the trajectory of the corresponding low Earth orbiting satellite. On the right (from top to bottom), there are intensities of waves in the hydrogen and helium bands from the data from TH-D (panels (a) and (b)) and TH-E (panels (c) and (d)) satellites and the intensities of proton fluxes measured by the MEPED and TED (panels (e)

and (f)) on a low Earth orbiting satellite. We used the TED data, because sometimes these data make it possible to better represent the spatial structure of the proton flux.

The NOAA-15 satellite in 1847–1853 UT crossed the latitude of EMIC wave detection immediately after the TH-E satellite stopped detecting waves at latitudes of 67°–68°, and the TH-D satellite began to enter the ion-cyclotron interaction region at latitudes of 70°–71° (Fig. 6). Each wave detection region in the latitudinal distribution of the fluxes of precipitating protons corresponds to a proton precipitation burst. A burst of protons with energies of 30–80 keV corresponding to a higher-latitude region of EMIC waves merges with the isotropic flux region, but an isolated burst in proton fluxes with energy of <20 keV (TED) can be clearly seen. The NOAA-16 passage also shows the existence of these precipitation regions at 1900–1905 UT (Fig. 7). The data from the NOAA-19 satellite at 1906–1913 UT (Fig. 8), as well as the NOAA-15 satellite at 1927–1931 UT (Fig. 9) and the NOAA-19 satellite at 1938–1945 UT (Fig. 10), show the presence of proton burst precipitations at a latitude of 70°–71°. The NOAA-16 satellite at 1941–1945 UT "sees" both EMIC wave generation regions almost at the same time (Fig. 11). It follows from Figs. 6–11 that both precipitation regions are visible when the low Earth orbiting satellite is at MLT > 17. During passages at MLT < 17, the satellite detects only precipitations at latitudes of 70°–71°. This can indicate the presence of two proton precipitation regions (ion-cyclotron interaction regions) with different longitude lengths on the TH-D and TH-E trajectories. Such structures can be observed in the evening sector in the plasmospheric tail region (for example, Yahnin et al., 2006).

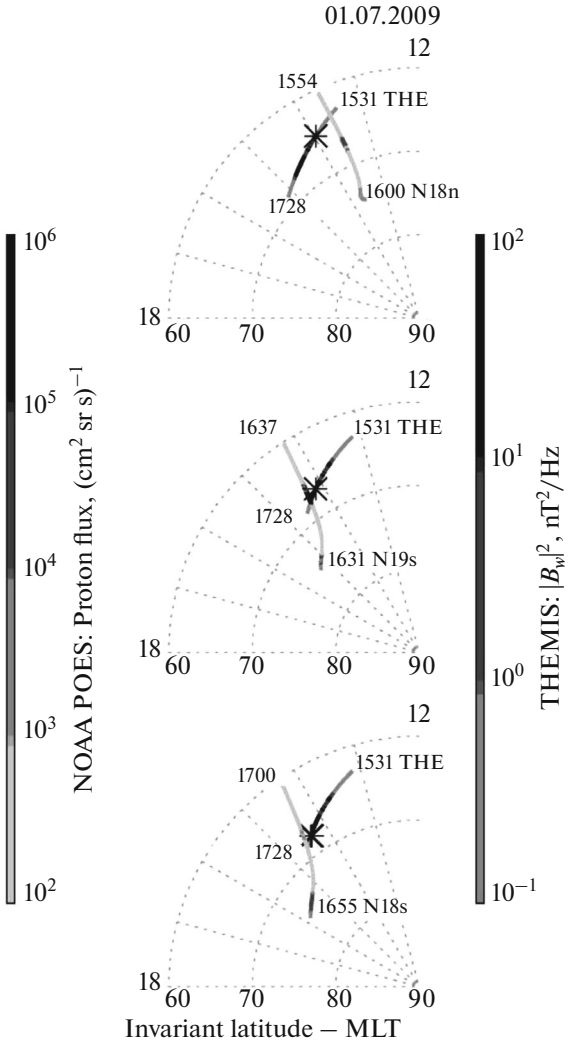


**Fig. 2.** Maps of trajectories in invariant latitude–MLT coordinates for THEMIS-E and POES (NOAA-18 and NOAA-19) satellites. Trajectories of low Earth orbiting satellites are shown for the intervals of 1554–1600 UT (NOAA-18), 1631–1637 UT (NOAA-19), and 1655–1700 UT (NOAA-18) on July 1, 2009. The asterisk on the THEMIS-E trajectory is the position of this satellite at the time of the passage of the low Earth orbiting satellite. Grayscale on the THEMIS-E trajectory shows the intensity of EMIC waves and on the POES trajectory, the flux of precipitating protons.

### *3.1.3. Event of February 8, 2009*

The generation of EMIC waves was detected by the TH-A and TH-E satellites in the midnight sector at a distance of 8–8.5$R_E$ with an interval of the order of half an hour (Fig. 12). Obviously, the position of the EMIC wave region did not change during this time. Three POES satellite passages are available for this event: NOAA-17 at 0258–0300 UT, NOAA-16 at 0318–0326 UT, and MetOp-02 at 0325–0329 UT in the interval of MLT = 2300–0030. All three passages fall on the period of intersection of the EMIC wave region with the TH-E satellite. The distributions of the proton fluxes in latitude are similar on all passages, and the region of EMIC waves coincides with the precipitation of protons at the equatorial edge of the isotropic fluxes (Fig. 13–15).

### *3.2. Conjugation Statistics of EMIC Wave Regions and Proton Precipitations*

Consideration of these and other events that satisfy the criteria selected above showed that proton precipitation was observed at the EMIC wave detection latitudes in most of the 157 examined cases. At the same time, the criteria that we used to select events do not mean that EMIC waves and proton precipitations are detected *simultaneously*. As can be seen from the given examples, the EMIC wave detection region can be very inhomogeneous and contain bursts and drops in the amplitude of the waves (e.g., TH-E satellite data in Fig. 3). It is interesting to compare the data of satellites in cases when POES crossed the latitude interval of interest to us *during* the detection of EMIC waves of sufficiently high intensity (for example, in the interval of ~1631–1637 UT on June 6, 2009, and ~1245–

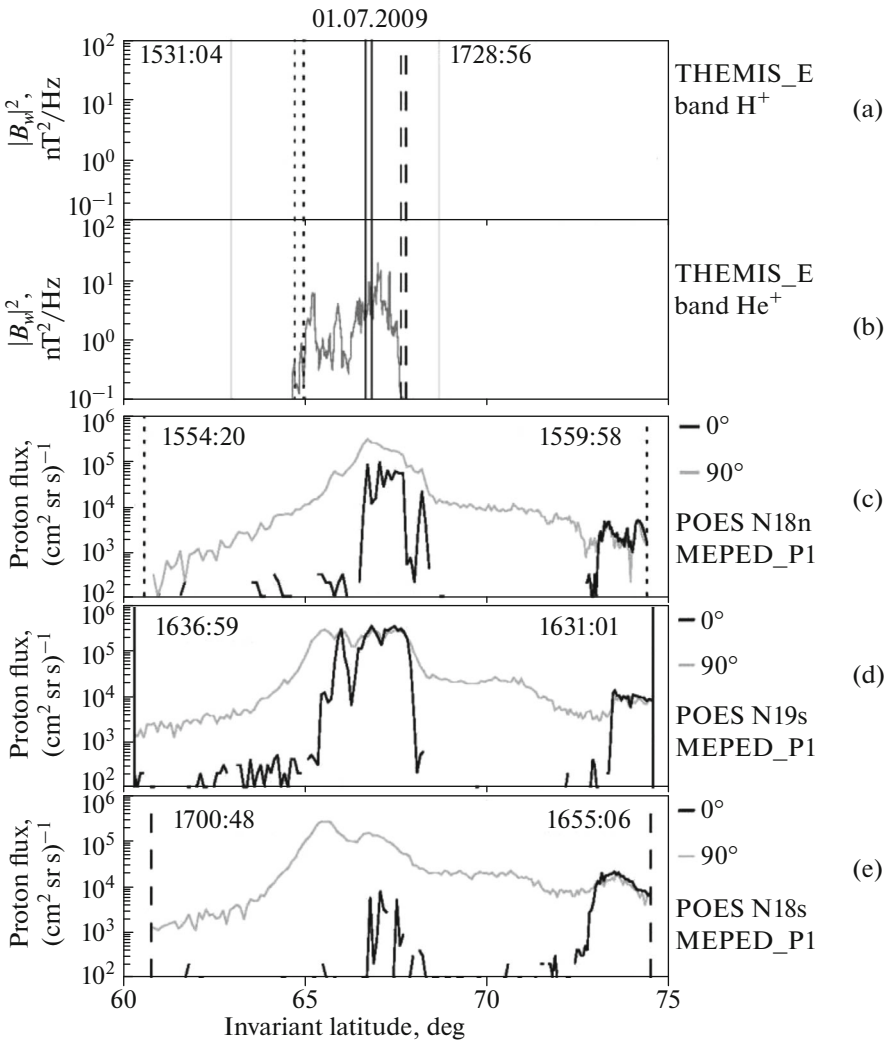


**Fig. 3.** Latitudinal intensity profiles of EMIC waves in the $H^+$ and $He^+$ bands (a, b), intensity profiles of the flux of trapped (gray line) and precipitating (black line) protons with energies of 30–80 keV (c, d, e) measured by NOAA-18 and NOAA-19 satellites during the three passages shown in Fig. 2. Gray vertical lines in (a) and (b) show the invariant latitudes of the THEMIS-E satellite at the beginning and at the end of the measurements of the waves shown in Fig. 1. The pair of vertical dashed lines in (a) and (b) mark the latitude range in which the THEMIS-E satellite was during the passage of NOAA-18 at ~1554–1600 UT, the data of which are shown in (c). A pair of vertical solid lines in (a) and (b) indicate the same but for the passage of NOAA-19 at 1631–1637 UT (data are given in (d)). The pair of vertical dashed lines in (a) and (b) mark the THEMIS-E position during the passage of NOAA-18 at ~1655–1701 UT (data are given in (e)).

1250 UT on July 1, 2009; Figs. 3 and 4). We found 68 such events when the wave intensity was higher than 1 $(nT)^2/Hz$. Analysis of these events showed that proton precipitations were observed in the conjugated region in 62 cases (~91%). The absence of precipitations in about ~9% of the events can apparently be due either to the errors in the magnetospheric magnetic field model or to the localization of the source of the EMIC wave region by MLT (recall that we are considering events in which satellites' MLT can differ up to 1 h).

## 4. DISCUSSION

From the consideration of examples of the relationship between generation regions of EMIC waves and proton precipitations, it follows that, when a low Earth orbiting satellite passes the conjugate region directly at the time of detection of EMIC waves by a magnetospheric satellite, it is most likely to detect precipitations of energetic protons. At the same time, there can be no detailed correspondence between EMIC wave regions and bursts (for example, Fig. 3). This is due to the fact that the region in which waves are generated can vary in time and space. Indeed, the generation of EMIC waves depends, in particular, on the intensity of the fluxes of energetic protons and their anisotropy (Kennel and Petschek, 1966). Variations of proton fluxes can be significantly modulated by substorm injections and nonstationary convection. Variations in the anisotropy of protons of the ring cur-

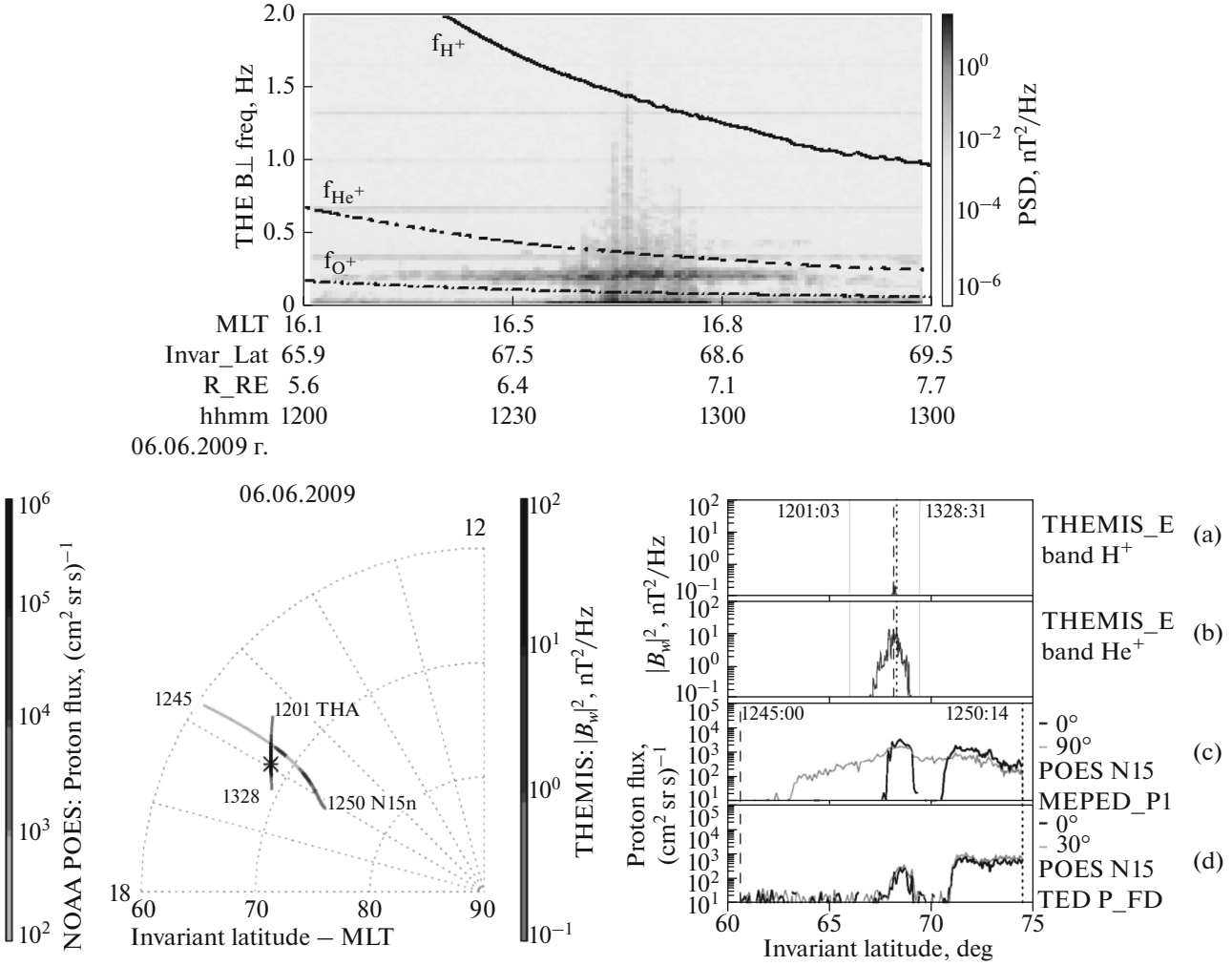


**Fig. 4.** Top: Spectrogram of the transverse fluctuations of the magnetic field measured by the THEMIS-A satellite at 1200–1330 UT on June 6, 2009. Bottom left: The THEMIS-A trajectory map (in the interval of 1201–1328 UT on June 6, 2009) and NOAA-15 (in the interval of 1245–1250 UT). The asterisk on the THEMIS-A trajectory marks the position of this satellite during the passage of NOAA-15. Bottom right: Latitudinal intensity profiles of EMIC waves in the $H^+$ and $He^+$ bands measured by the THEMIS-A satellite (in (a) and (b)), fluxes of captured and precipitating protons with energies of 30–80 keV from the MEPED according to the data from the NOAA-15 satellite (c), fluxes of precipitating protons with energy <20 keV according to the data from the TED (d). Vertical dashed and dotted lines in (a) and (b) mark the latitude range in which the THEMIS-A satellite was during the passage of NOAA-15 at ~1245–1250 UT.

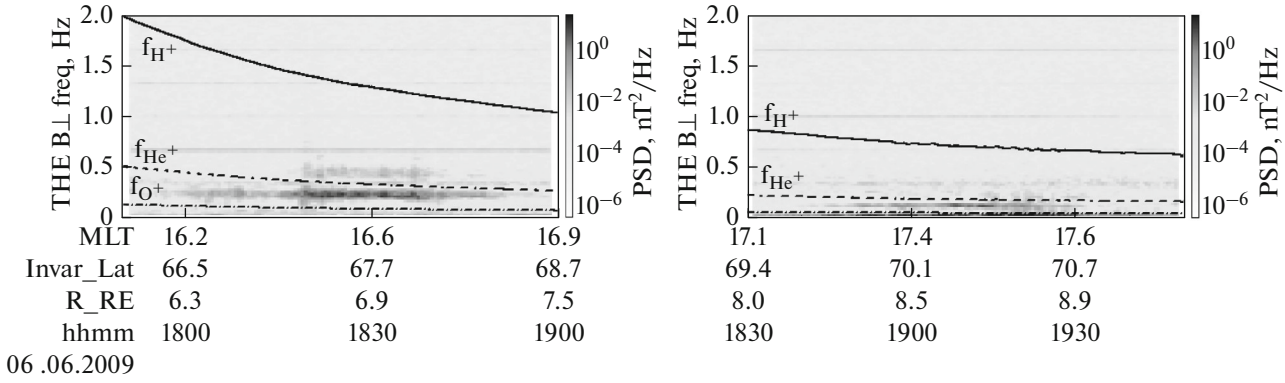


**Fig. 5.** Spectrograms of the transverse fluctuations of the magnetic field measured on June 6, 2009, by the satellites THEMIS-E at 1750–1900 UT (left) and THEMIS-D at 1830–1950 UT (right).

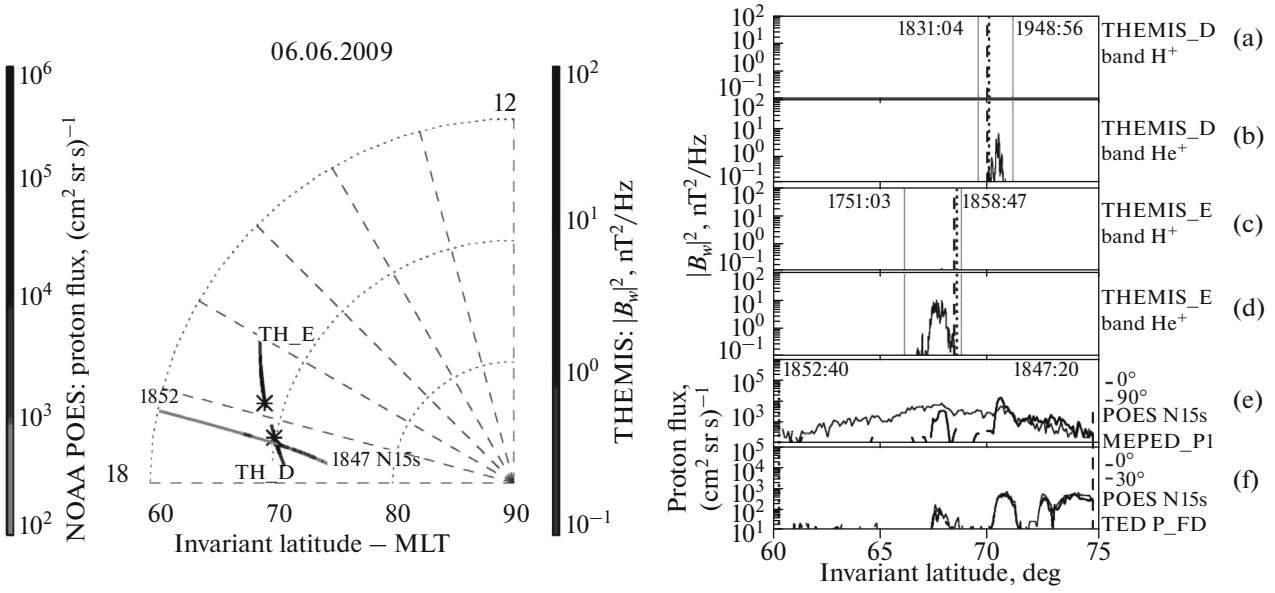


**Fig. 6.** Left: Trajectory map of THEMIS-E (in the interval of 1751–1859 UT on June 6, 2009), THEMIS-D (in the interval of 1831–1949 UT), and NOAA-15 (in the interval of 1847–1852 UT). The asterisks on the trajectories of THEMIS-D and -E mark positions of these satellites during the passage of NOAA-15. Right: Latitudinal intensity profiles of EMIC waves in the $H^+$ and $He^+$ bands measured by the THEMIS-D and -E satellites (a, b, c, d), fluxes of trapped and precipitating protons with energies of 30–80 keV according to the MEPED on the NOAA-15 satellite (e), and the fluxes of precipitating protons with energies of <20 keV according to the TED (f). Vertical dashed and dotted lines in (a) and (b) ((c) and (d)) indicate the position of the THEMIS-D (THEMIS-E) satellite during the passage of the NOAA-15 satellite.

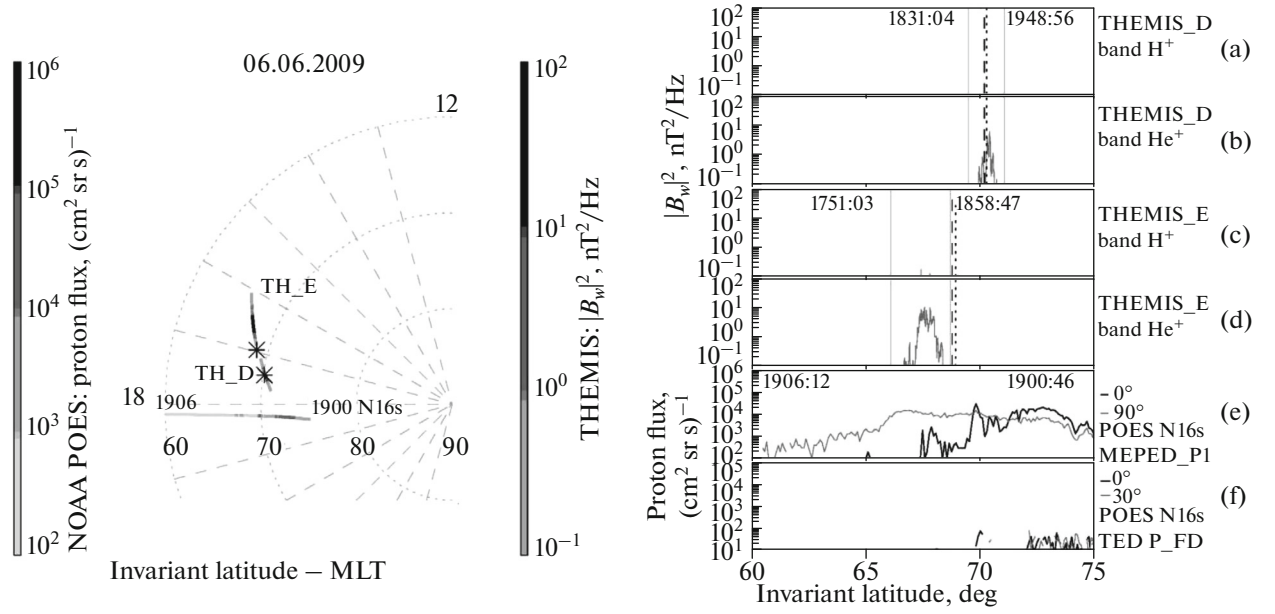


**Fig. 7.** The same as in Fig. 6 but for the passage of the NOAA-16 low Earth orbiting satellite at ~1900–1906 UT.

rent are closely related to the variability of the solar wind pressure (for example, Olson and Lee, 1981). In addition, the solar wind pressure affects the day–night asymmetry in the magnetosphere and, thus, the anisotropy radial distribution due to the effect of splitting of drift shells (Roederer, 1967; Wang et al., 2012). The "visualization" of the spatiotemporal variability of the EMIC wave generation region was illustrated by Yahnina et al. (2008, Fig. 1), where the dynamics of daytime proton auroras (bursts) and EMIC waves associated with them were considered. Figure 3 in this paper also confirms the variability of proton precipita-

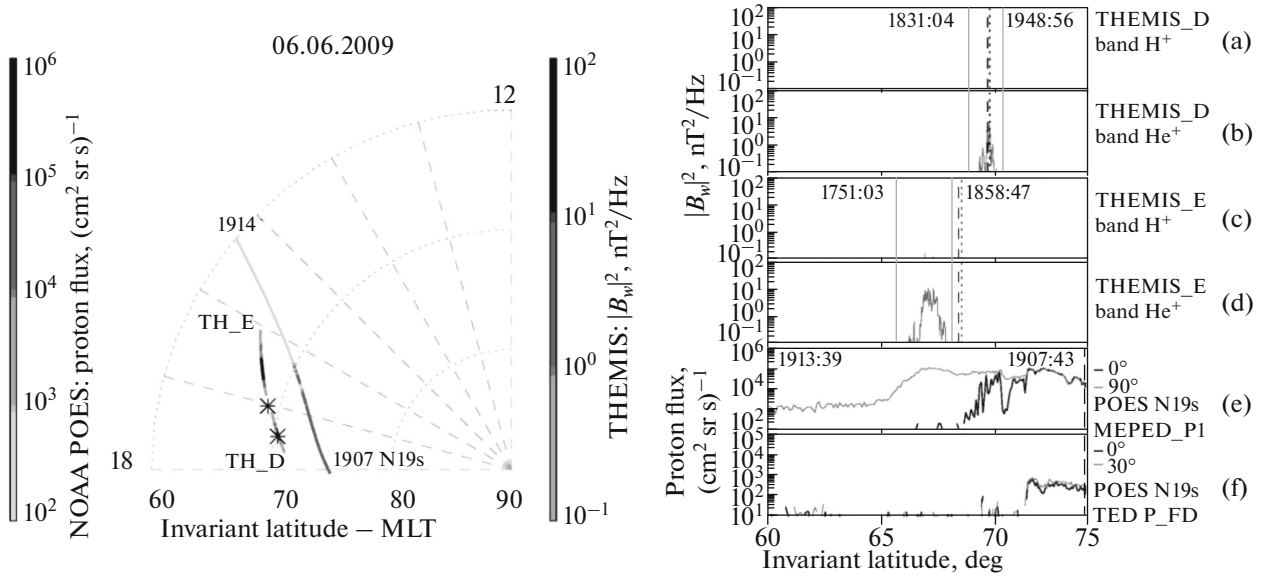


**Fig. 8.** The same as in Fig. 6 but for the passage of the NOAA-19 low Earth orbiting satellite at ~1907–1914 UT.

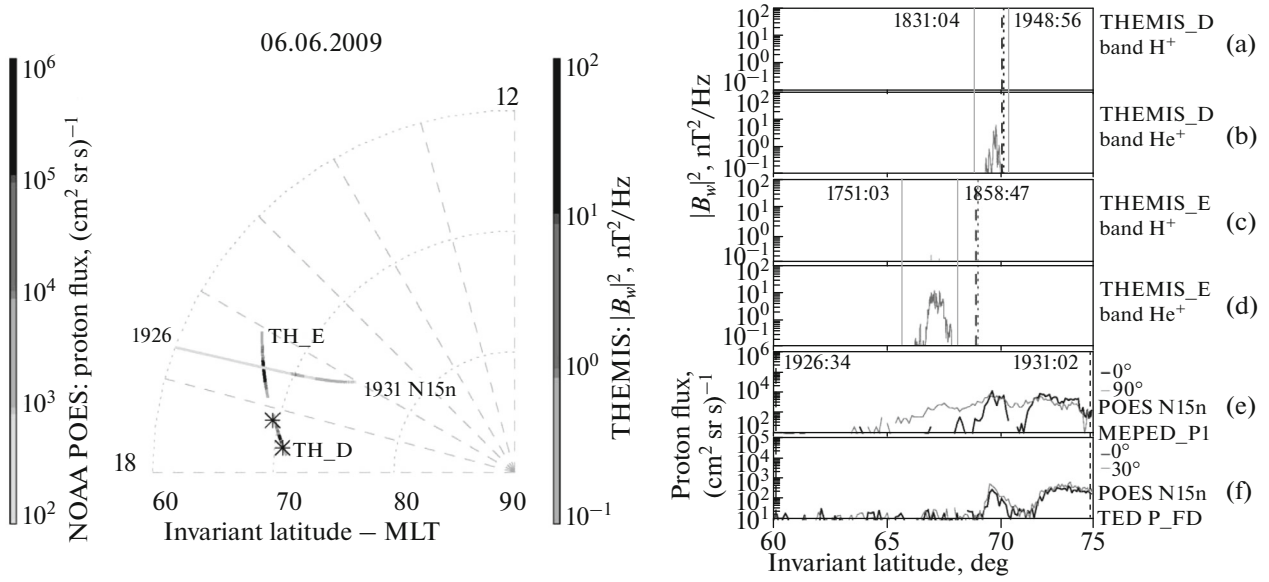


**Fig. 9.** The same as in Fig. 6 but for the passage of the NOAA-15 low Earth orbiting satellite at ~1926–1931 UT.

tions in the daytime sector (see also Fig. 9 in Engebretson et al., 2015 and Fig. 3 in Yahnin et al., 2015).

Since the magnetospheric satellite crosses the wave generation region over a long period of time, both spatial and temporal variations contribute to its measurements. The advantage of low Earth orbiting observations is that the satellite at low altitudes scans very quickly a large range of latitudes (in a few minutes) and gives an instantaneous section of the studied region, and the sequence of such passages makes it possible to track the temporal dynamics of the ion-cyclotron interaction region. The relationship between EMIC wave generation and proton precipitation regions shown here (Morley et al., 2009; Usanova et al., 2010), as well as the similarity of the spatial distributions of the probability of observing EMIC waves (Usanova et al., 2012; Keika et al., 2013) and precipitations of energetic protons (Semenova et al., 2017), indicate the possibility of remote diagnostics of ion-cyclotron instability in the magnetosphere from low Earth orbiting satellites.

As already noted, the transverse pitch-angle anisotropy of energetic protons is necessary for the development of ion-cyclotron instability. This means

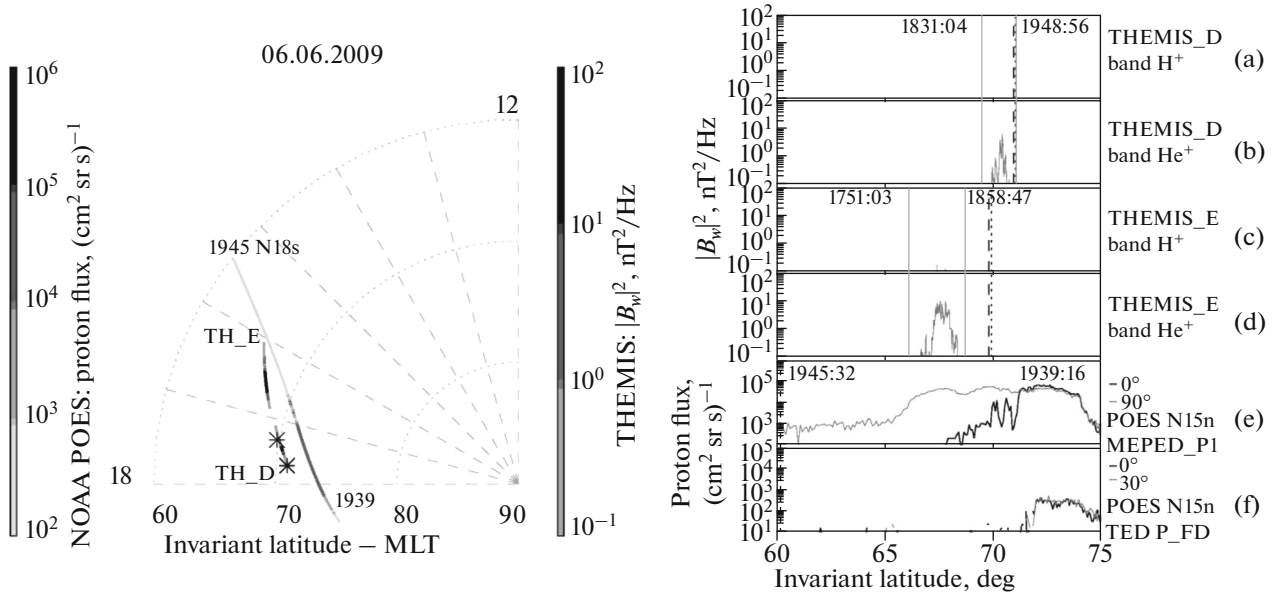


**Fig. 10.** The same as in Fig. 6 but for the passage of the NOAA-18 low Earth orbiting satellite at ~1939–1945 UT.

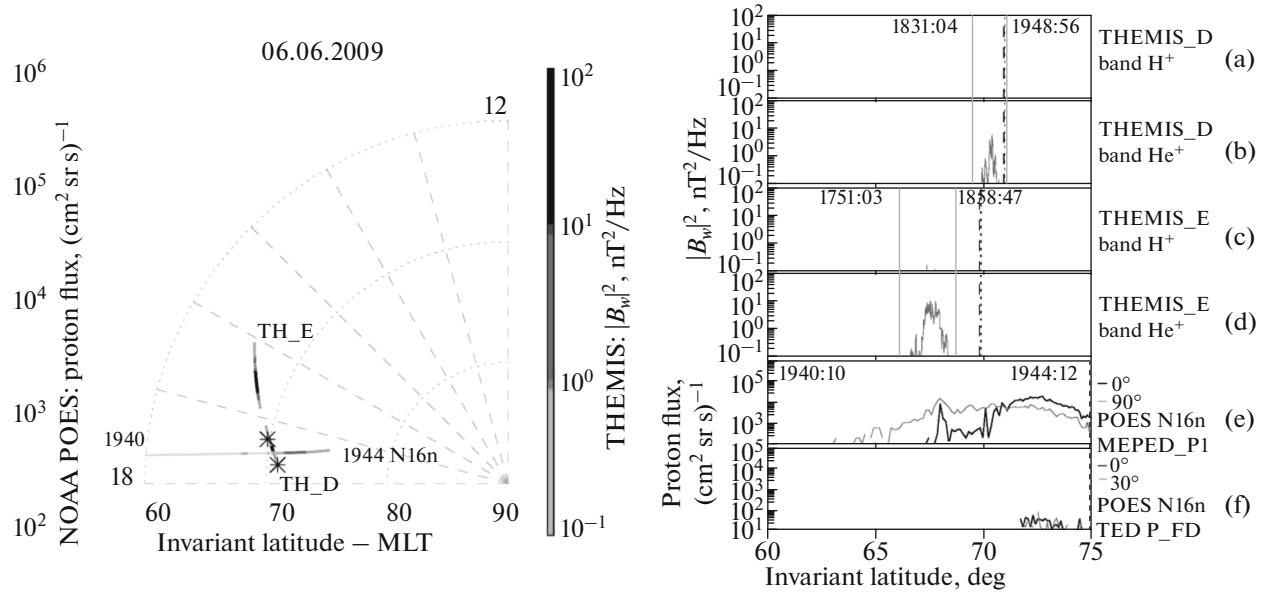


**Fig. 11.** The same as in Fig. 6 but for the passage of the NOAA-16 low Earth orbiting satellite at ~1940–1944 UT.

that EMIC waves and associated proton precipitation should be observed in the region of anisotropic proton fluxes to the equator from the isotropic zone boundary. Poleward from this boundary, proton fluxes are isotropic because of the violation of the adiabaticity of motion and scattering of particles in the region where a certain relationship exists between the radius of curvature of the lines of force and the Larmor radius of the particle (Sergeev and Tsyganenko, 1982). This is the so-called scattering on the current sheet. The assumption about this mechanism for the formation of the isotropic boundary is an important element in the method of identifying the configuration of the magnetic field of the magnetosphere based on data from low Earth orbiting satellites (Sergeev and Gvozdevsky, 1995; Newell et al., 1998). However, the characteristics of the magnetic field in the region of the magnetospheric projection of the isotropic boundary quite often do not correspond to the criterion for the scattering of energetic protons on the current sheet. This conclusion was reached, for example, by Sergeev et al. (2015a), who designed the boundaries of isotropic

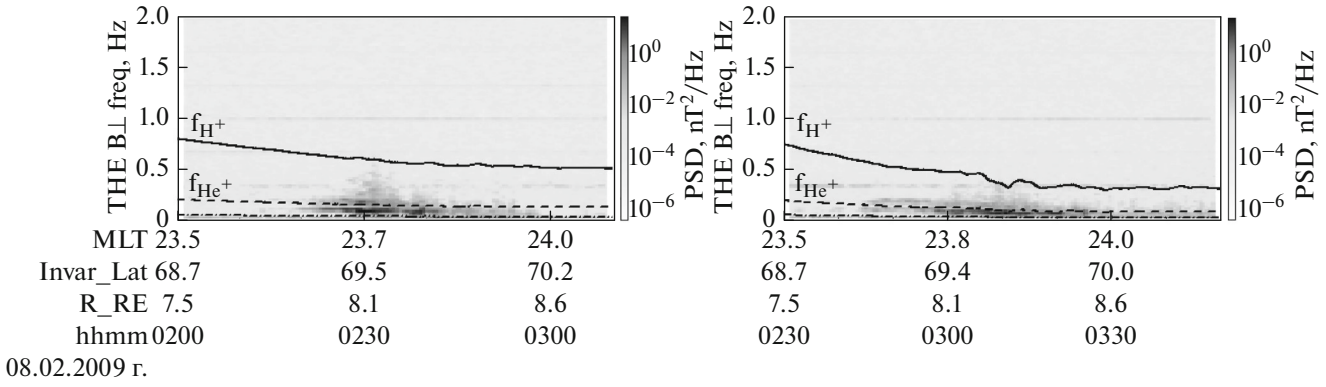


**Fig. 12.** Spectrograms of the transverse fluctuations of the magnetic field measured at 0200–0310 UT and 0230–0350 UT on Feb. 8, 2009, by the THEMIS-A and THEMIS-E satellites, respectively.

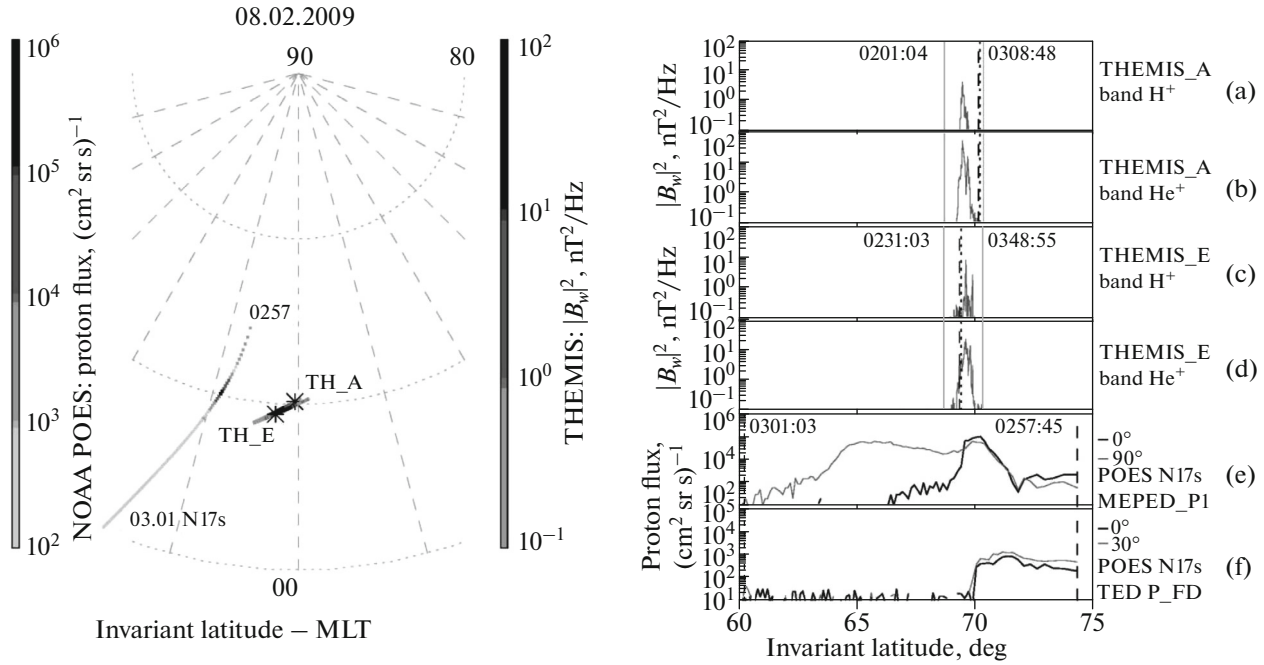


**Fig. 13.** The same as in Fig. 6 but for the THEMIS-A satellites (in the interval of 0201–0309 UT on Feb. 8, 2009) and THEMIS-E (in the interval of 0231–0349 UT) as well as for the passage of the NOAA-17 low Earth orbiting satellite at ~0257–0301 UT.

fluxes (observed from low Earth orbiting satellites) to the magnetosphere using an adaptive magnetic field model based on magnetic measurements on the THEMIS satellites. These authors suggested that the discrepancy can be due to proton scattering by EMIC waves. The possibility of a shift in the isotropic boundary due to scattering by EMIC waves is indirectly indicated by the results of earlier works (Sergeev et al., 2015b; Ilie et al., 2015). The results of conjugate observations of the fluxes of energetic protons at low altitudes and waves in the magnetosphere shown in Figs. 6 and 13–15 in our paper indicate that, if the IC instability region in the anisotropic zone is adjacent to the boundary of isotropic fluxes, then the proton precipitations caused by it can indeed complicate the determination of the isotropic boundary formed by the particle scattering mechanism on the current sheet.

## 5. CONCLUSIONS

The conjugacy of the regions of EMIC wave observation and energetic proton precipitations is experimental confirmation of the theoretical loss cone filling concepts and energetic proton precipitations during the generation of EMIC waves. This conjugacy means that it is possible to identify the regions of development of ion-cyclotron instability in the magnetosphere from observations of proton precipitations by low Earth orbiting satellites.

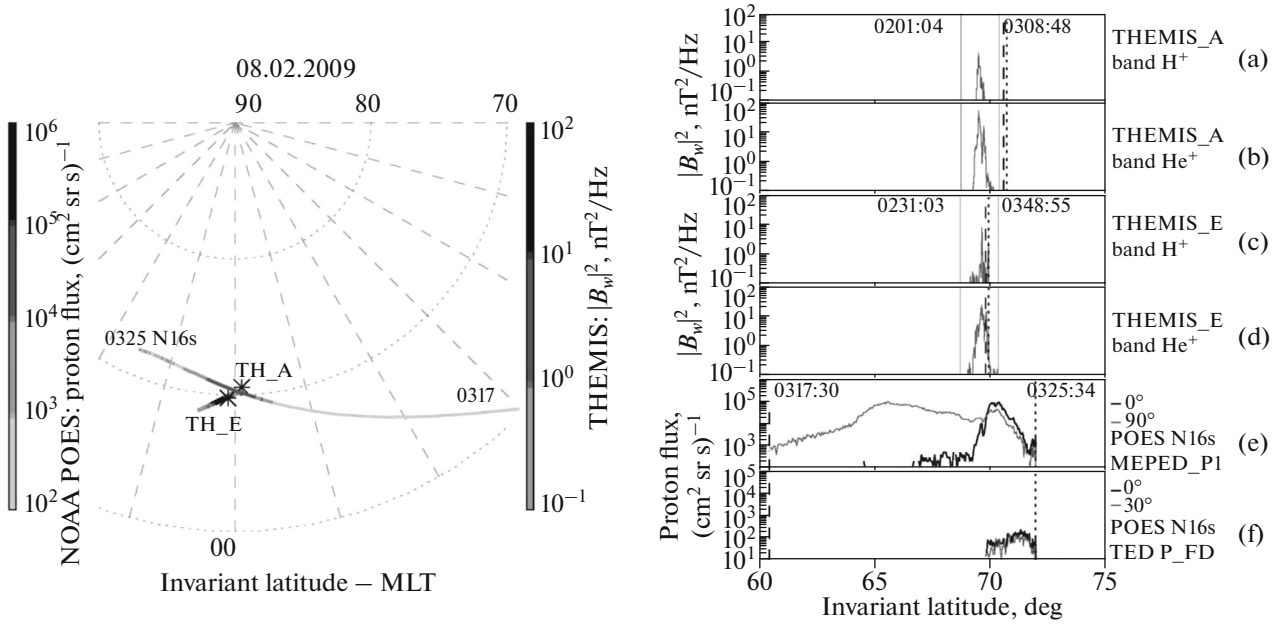


**Fig. 14.** The same as in Fig. 13 but for the passage of the NOAA-16 low Earth orbiting satellite at ~0317–0325 UT.

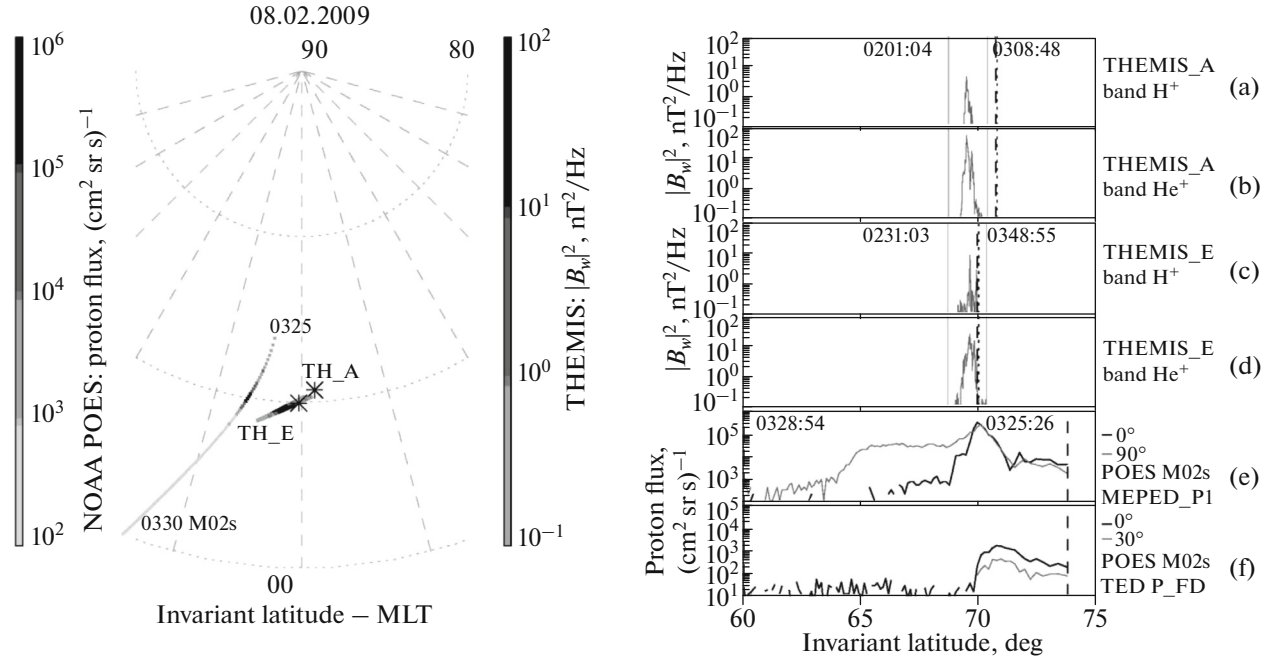


**Fig. 15.** The same as in Fig. 13 but for the passage of the MetOp-02 low Earth orbiting satellite at ~0325–0329 UT.

The data from magnetospheric satellites often does not make it possible to distinguish between the spatial and temporal variations in EMIC wave generation region. Data from low Earth orbit satellites give almost instantaneous sections of precipitations from this region and, thus, give an idea of the instantaneous spatial structure of the EMIC interaction region. Successive passages of low Earth orbiting satellites make it possible to analyze the temporary changes in this structure.

The flux of precipitating protons associated with the generation region of EMIC waves can mask the position of the isotropic flux boundary due to the scattering of particles on the current sheet, thereby shifting the isotropic proton boundary to the equator.

## ACKNOWLEDGMENTS

We thank the THEMIS Project Team (project manager V. Angelopoulos) for providing free access to project data (http://themis.ssl.berkeley.edu), and NOAA for providing POES satellite data (https://www.ngdc.noaa.gov/stp/satellite/poes/dataaccess.html). This work was supported by the Russian Science Foundation, project no. 15-12-20005.

## REFERENCES

Angelopoulos, V., The THEMIS mission, *Space Sci. Rev.*, 2008, vol. 141, pp. 5–34, doi 10.1007/s11214-008-9336-1

Auster, H.U., Glassmeier, K.H., Magnes, W., et al., The THEMIS fluxgate magnetometer, *Space Sci. Rev.*, 2008, vol. 141, pp. 235–264. doi 10.1007/s11214-008-9365-9

Bespalov, P.A., Demekhov, A.G., Grafe, A., and Trakhtengerts, V.Yu., On the role of collective interactions in asymmetric ring current formation, *Ann. Geophys.*, 1994, vol. 12, pp. 422–430.

Cornwall, J.M., Coroniti, F.V., and Thorne, R.M., Turbulent loss of ring current protons, *J. Geophys. Res.*, 1970, vol. 75, pp. 4699–4709.

Engebretson, M.J., Posch, J.L., Wygant, J.R., et al., Van Allen probes, NOAA, GOES, and ground observations of an intense EMIC wave event extending over 12 h in magnetic local time, *J. Geophys. Res.: Space Phys.*, 2015, vol. 120, pp. 5465–5488. doi 10.1002/2015JA021227

Erlandson, R.E. and Ukhorskiy, A.J., Observations of electromagnetic ion cyclotron waves during geomagnetic storms: Wave occurrence and pitch angle scattering, *J. Geophys. Res.*, 2001, vol. 106, pp. 3883–3895.

Evans, D.S. and Greer, M.S., *Polar Orbiting Environmental Satellite Space Experiment Monitor-2: Instrument Description and Archive Data Documentation, NOAA Technical Memorandum Version 1.3*, Boulder, Colorado: NOAA Environmental Center, 2004.

Ilie, R., Ganushkina, N., Toth, G., Dubyagin, S., and Liemohn, M.W., Testing the magnetotail configuration based on observations of low-altitude isotropic boundaries during quiet times, *J. Geophys. Res.: Space Phys.*, 2015, vol. 120, pp. 10557–10573. doi 10.1002/2015JA021858

Keika, K., Takahashi, K., Ukhorskiy, A.Y., and Miyoshi, Y., Global characteristics of electromagnetic ion cyclotron waves: Occurrence rate and its storm dependence, *J. Geophys. Res.: Space Phys.*, 2013, vol. 118, pp. 4135–4150. doi 10.1002/jgra.50385

Kennel, C.F. and Petschek, H.E., Limit on stably trapped particle fluxes, *J. Geophys. Res.*, 1966, vol. 71, no. 1, pp. 1–28.

Li, W., Ni, B., Thorne, R.M., et al., Quantifying hiss-driven energetic electron precipitation: a detailed conjunction event analysis, *Geophys. Res. Lett.*, 2014, vol. 41, pp. 1085–1092. doi 10.1002/2013GL059132

Morley, S.K., Ables, S.T., Sciffer, M.D., and Fraser, B.J., Multipoint observations of Pc1–2 waves in the afternoon sector, *J. Geophys. Res.*, 2009, vol. 114, A09205. doi 10.1029/2009JA014162

Newell, P.T., Sergeev, V.A., Bikkuzina, G.R., and Wing, S., Characterizing the state of the magnetosphere: Testing the ion precipitation maxima latitude (b2i) and the ion isotropy boundary, *J. Geophys. Res.*, 1998, vol. 103, pp. 4739–4745.

Olson, J.V. and Lee, L.C., Pc1 wave generation by sudden impulses, *Planet. Space Sci.*, 1983, vol. 31, pp. 295–302.

Roederer, J.G., On the adiabatic motion of energetic particles in a model magnetosphere, *J. Geophys. Res.*, 1967, vol. 72, pp. 981–992.

Sagdeev, R.Z. and Shafranov, V.D., On the Instability of a plasma with an anisotropic distribution of velocities in a magnetic field, *Sov. Phys. JETP*, 1961, vol. 12, no. 1, pp. 130–132.

Semenova, N.V., Yahnina, T.A., Yahnin, A.G., and Demekhov, A.G., Global distribution of energetic proton precipitations equatorward of the boundary of isotropic fluxes, *Geomagn. Aeron. (Engl. Transl.)*, 2017, vol. 57, no. 4, pp. 398–405.

Sergeev, V.A. and Gvozdevsky, B.B., MT-index—a possible new index to characterize the magnetic configuration of magnetotail, *Ann. Geophys.*, 1995, vol. 13, pp. 1093–1103. doi 10.1007/s00585-995-1093-9

Sergeev, V.A. and Tsyganenko, N.A., Energetic particle losses and trapping boundaries as deduced from calculations with a realistic magnetic field model, *Planet. Space Sci.*, 19892, vol. 30, pp. 999–1006. doi 10.1016/0032-0633(82)90149-0

Sergeev, V.A., Chernyaev, I.A., Angelopoulos, V., and Ganushkina, N.Y., Magnetospheric conditions near the equatorial footpoints of proton isotropy boundaries, *Ann. Geophys.*, 2015a, vol. 33, pp. 1485–1493. doi 10.5194/angeo-33-1485-2015

Sergeev, V.A., Chernyaeva, S.A., Apatenkov, S.V., Ganushkina, N.Y., and Dubyagin, S.V., Energy-latitude dispersion patterns near the isotropy boundaries of energetic protons, *Ann. Geophys.*, 2015b, vol. 33, pp. 1059–1070.

Tsyganenko, N.A., A magnetospheric magnetic field model with a warped tail current sheet, *Planet. Space Sci.*, 1989, vol. 37, pp. 5–20.

Usanova, M.E., Mann, I.R., Kale, Z.C., et al., Conjugate ground and multisatellite observations of compression-related EMIC Pc1 waves and associated proton precipitation, *J. Geophys. Res.*, 2010, 2010, vol. 115, A07208. doi 10.1029/2009JA014935

Usanova, M.E., Mann, I.R., Bortnik, J., Shao, L., and Angelopoulos, V., THEMIS observations of electromagnetic ion cyclotron wave occurrence: Dependence on AE, SYMH, and solar wind dynamic pressure, *J. Geophys. Res.*, 2012, vol. 117, A10218. doi 10.1029/2012JA018049

Wang, C.P., Zaharia, S.G., Lyons, L.R., and Angelopoulos, V., Spatial distributions of ion pitch angle anisotropy in the near-Earth magnetosphere and tail plasma sheet, *J. Geophys. Res.*, 2012, vol. 118, pp. 244–255. doi 10.1029/2012JA018275

Yahnin, A.G. and Yahnina, T.A., Energetic proton precipitation related to ion-cyclotron waves, *J. Atmos. Sol.-*

*Terr. Phys.*, 2007, vol. 69, no. 14, pp. 1690–1706. doi 10.1016/j.jastp.2007.02.010

Yahnin, A.G., Yahnina, T.A., Ganushkina, N.Y., Angelopoulos, V., Mozer, F.S., Kangas, J., Manninen, J., Fritz, T.A., and Russell, C.T., Multi-satellite study of phenomena in the evening magnetosphere during the Pc1–2 event, in *Proc. of XXV Apatity Seminar "Physics of Auroral Phenomena", 26 February–1 March, 2002, Apatity, Russia*, 2002, pp. 85–88.

Yahnin, A.G., Yahnina, T.A., and Demekhov, A.G., Interrelation between localized energetic particle precipitation and cold plasma in homogeneities in the magnetosphere, *Geomagn. Aeron. (Engl. Transl.)*, 2006, vol. 46, no. 3, pp. 332–338.

Yahnin, A.G., Popova, T.A., and Yahnina, T.A., Some characteristics of the magnetospheric source of dayside subaroural proton precipitations during magnetospheric compression, *Cosmic Res.*, 2015, vol. 53, no. 1, pp. 80–87.

Yahnina, T.A., Yahnin, A.G., Kangas, J., et al., Energetic particle counterparts for geomagnetic pulsations of Pc1 and IPDP types, *Ann. Geophys.*, 2003, vol. 21, pp. 2281–2292.

Yahnina, T.A., Frey, H.U., Bosinger, T., and Yahnin, A.G., Evidence for subauroral proton flashes on the dayside as the result of the ion cyclotron interaction, *J. Geophys. Res.*, 2008, vol. 113, A07209. doi 10.1029/2008JA013099

*Translated by O. Pismenov*